Korean J. Chem. Eng., 38(8), 1556-1565 (2021)
DOI: 10.1007/s11814-021-0828-y

pISSN: 0256-1115
eISSN: 1975-7220

Optimization of basic magenta adsorption onto Fe/Cu nanocomposites synthesized by sweet potato leaf extract using response surface methodology

Yuanyuan Niu*,‡, Ruijuan Jia*,‡, Chenglin Liu*, Xiuli Han*,,†, Chun Chang*,**, and Junying Chen*,****

*School of Chemical Engineering, Zhengzhou University, Zhengzhou 450001, China
**Henan Center for Outstanding Overseas Scientists, Zhengzhou 450001, China
(*Received 8 December 2020 • Revised 15 February 2021 • Accepted 29 April 2021*)

Abstract−Green synthesis of metal nanoparticles using plant extracts as an effective bio-reducing reagent has attracted considerable attention. Fe/Cu nanocomposites synthesized by extracts of sweet potato leaves served to remove basic magenta (BM) from aqueous solution. The adsorption operation conditions of BM on Fe/Cu nanocomposites were optimum by Box-Behnken design (BBD) model of response surface methodology (RSM). The adsorption equilibrium data were well described by the Sips and Redlich-Peterson models. The thermodynamic studies showed that the adsorption process was endothermic and spontaneous. The maximum adsorption capacity from the Sips model was 235.92 mg/g at 298 K, which indicated that Fe/Cu nanocomposites had potential application in wastewater treatment. As indicated by pseudo-second order kinetics model, the adsorption of BM onto Fe/Cu nanocomposites could be achieved through the complexation, H-bonding, π-π adsorbate-adsorbent interaction, and electrostatic interaction at different pH values.

Keywords: Sweet Potato Leaf, Fe/Cu Nanocomposites, Basic Magenta, Adsorption, Response Surface Methodology

INTRODUCTION

Synthetic dyes are widely used in many industries, such as food, paper, plastics, leather, and textiles [1-4]. It is estimated that more than 7×10^5 tons of dye are produced every year [5,6]. Most dyes are teratogenic, carcinogenic and mutagenic, which has toxic effects on animals and humans [7-9]. Hence, adequate treatment of dye wastewater is of great significance to human health and environmental quality.

Many technologies are applied to wastewater treatment, such as adsorption [10], chemical oxidation [11], biodegradation [12], extraction [13] and membrane filtration [14]. From the these techniques, adsorption is considered as an economical method due to high removal capacity, low cost and operational simplicity. BM is a cationic dye which has higher brilliance and color intensity, it is hard to remove and has a carcinogenic effect, so it is important to remove basic magenta (BM) from wastewater. Nowadays, chitosan/montmorillonite intercalated composite, activated carbon, and nanotubes as adsorbents are used to remove the dye in the wastewater [15-17].

Nanoparticles as adsorbents are gaining great interest in wastewater treatment. The advantages of nanoparticles used for environmental remediation include high adsorption rate and stability. The traditional synthesis methods are generally costly and involve chemical substances, such as $NaBH_4$ and organic solvents, and the chemicals are corrosive and flammable. The green synthesis method of metal nanomaterials using plant extracts is simple and eco-friendly [18], because the plant extracts contain phenols and flavonoids which can reduce metal ions without additional chemical reagent. Now, several plant extracts such as garlic vine leaf, centella asiatica, grape leaf and green tea have been successfully used in the synthesis of metal nanomaterials [19-22].

In this work, the Fe/Cu nanocomposites were synthesized using extracts of sweet potato leaf and used as an adsorbent to remove BM from aqueous solution. The adsorption conditions of BM onto Fe/Cu nanocomposites were optimized by response surface methodology (RSM). The adsorption isotherms, kinetics and mechanism were systematically investigated.

EXPERIMENTAL MATERIALS AND METHODS

1. Materials

Sweet potato leaves were collected from Zhengzhou in Henan province, China. Ferric chloride hexahydrate ($FeCl_3\cdot6H_2O$), cupric chloride dehydrate ($CuCl_2\cdot2H_2O$), and citric acid monohydrate ($C_6H_8O_7\cdot H_2O$) were all purchased from Sinopharm Chemical Reagent Co. Ltd. They were all analytical grade. The BM stock solution (500 mg/L) was prepared with deionized water and stored at 4 °C in the refrigerator.

2. Preparation of Sweet Potato Leaf Extracts

Sweet potato leaves were thoroughly washed using deionized water and exposed to the sun-dry until the quality no longer changed, then the leaves were cut into small pieces. Subsequently, the dried sweet potato leaves were added to deionized water at a concentration of 60 g/L, and the temperature was raised to 363 K for 150 min. The treated extracts were centrifuged for 30 min at 4,200 rpm to obtain clear supernatant. The supernatant was stored at 277 K in

†To whom correspondence should be addressed.
E-mail: xlhan@zzu.edu.cn
‡These authors contributed equally to this work.

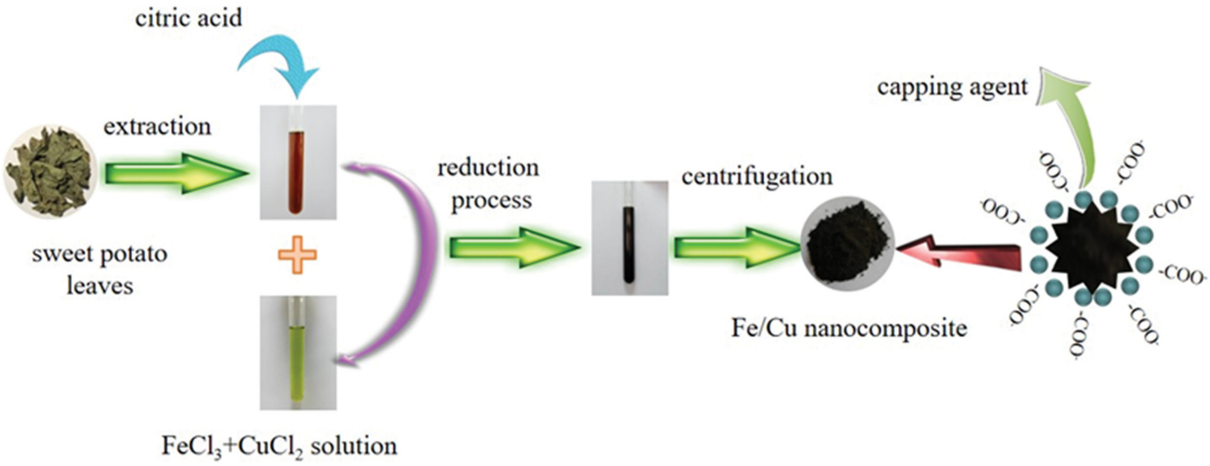

Fig. 1. Schematic illustration for the synthesis of Fe/Cu nanocomposites.

the refrigerator prior to being used.

3. Synthesis of Fe/Cu Nanocomposites

The synthesis process of Fe/Cu nanocomposites is shown in Fig. 1. Citric acid monohydrate (0.002 mol) was added to 500 mL beaker which already contained 160 mL sweet potato leaf extract. Subsequently, 80 mL $CuCl_2$ and $FeCl_3$ mixed solution (0.12 mol/L) at a molar ratio of 1 : 1 was added dropwise to the extract solution under continuous stirring for 180 min at ambient temperature. The resulting product, namely Fe/Cu nanocomposites, was separated by centrifugation at 4,200 rpm for 30 min and subsequently the precipitate was washed with deionized water three times. Finally, the sample was dried in the oven at 333 K for 480 min.

4. Adsorption Experiments

The adsorption capacity of BM on Fe/Cu nanocomposites was studied by several batch experiments. The effects of the time, adsorbent dosage and pH on the adsorption capacity were investigated. First, a certain amount of Fe/Cu nanocomposites was put into a 50 mL Erlenmeyer flask, and then 20 mL BM solution with the desired concentration was added. The pH value of the BM solution was adjusted by 0.1 mol/L HCl or NaOH. The flasks were sealed with plastic wrap and placed in air batch shaker at 130 rpm for the preselected time intervals. In each adsorption experiment, the concentration of BM was measured using UV-Vis spectrophotometry at 542 nm (TU-1810, CN).

The equilibrium adsorption capacity q_e (mg/g) of BM is calculated using the following equation:

$$q_e = \frac{(C_0 - C_e)V}{m} \quad (1)$$

where C_0 (mg/L) and C_e (mg/L) are the initial and equilibrium concentrations of BM, respectively. V (L) is the volume of BM solution, and m (g) represents the mass of Fe/Cu nanocomposites.

5. Characterization

The characteristics of Fe/Cu nanocomposites were determined by scanning electron microscopy (SEM, FEI Quanta 200), energy dispersive X-ray spectroscopy (EDS, FEI Quanta 200), X-ray photoelectron spectroscopy (XPS, Thermo ESCALAB 250XI), Fourier transform infrared spectroscopy (FTIR, PE-1710, USA). Nitrogen adsorption/desorption isotherms were measured at 77 K by surface area analyzer (JW-BK132F, CN). Specific surface areas were calculated according to the Brunauer-Emmett-Teller (BET) equation.

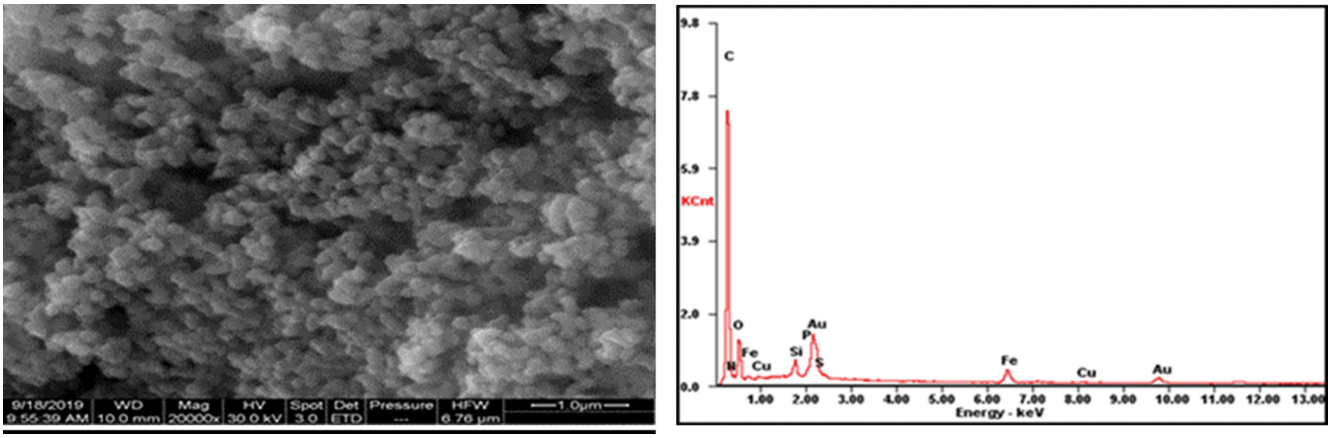

Fig. 2. SEM micrograph and EDS spectra of Fe/Cu nanocomposites.

RESULTS AND DISCUSSION

1. Characterization of the Fe/Cu Nanocomposites

The Fe/Cu nanocomposites were sputtered with gold before SEM observation. The SEM and EDS images of Fe/Cu nanocomposites are shown in Fig. 2. It is clear that Fe/Cu nanocomposites were granular and most of them were spherical. The average particle sizes of Fe/Cu nanocomposites ranged from 150 to 500 nm. Notably, the Fe/Cu nanocomposites had a certain agglomeration phenomenon. It was probably due to the sweet potato leaf extract being a mixture of various natural compounds, and the polyphenols and flavanols may affect the aggregation of the material during preparation [23]. The EDS spectrum contains the peaks of C, O, Fe, Cu and N etc., proving the presence of Fe and Cu on the nanocomposites. The C and O signals mainly stem from the polyphenol groups and other C, O-containing molecules. Therefore, the polyphenols contained in sweet potato leaves played a crucial role in the synthesis of Fe/Cu nanocomposites.

XPS spectra of Fe/Cu nanocomposites are shown in Fig. 3. There were three distinct peaks in the C 1s curves, the peaks at 284.5, 286.3 and 288.6 eV can be considered as C=C, C-OH and C=O, respectively. These signals may come from polyphenol groups and citric acid in the Fe/Cu nanocomposites [22]. Signals at around 531.4 and 532.8 eV (Fig. 3(b)) represent the presence of Fe-O/Cu-O and O=C-OH functional groups, respectively [24]. The presence of C1s and O1s in the sample means that some biological

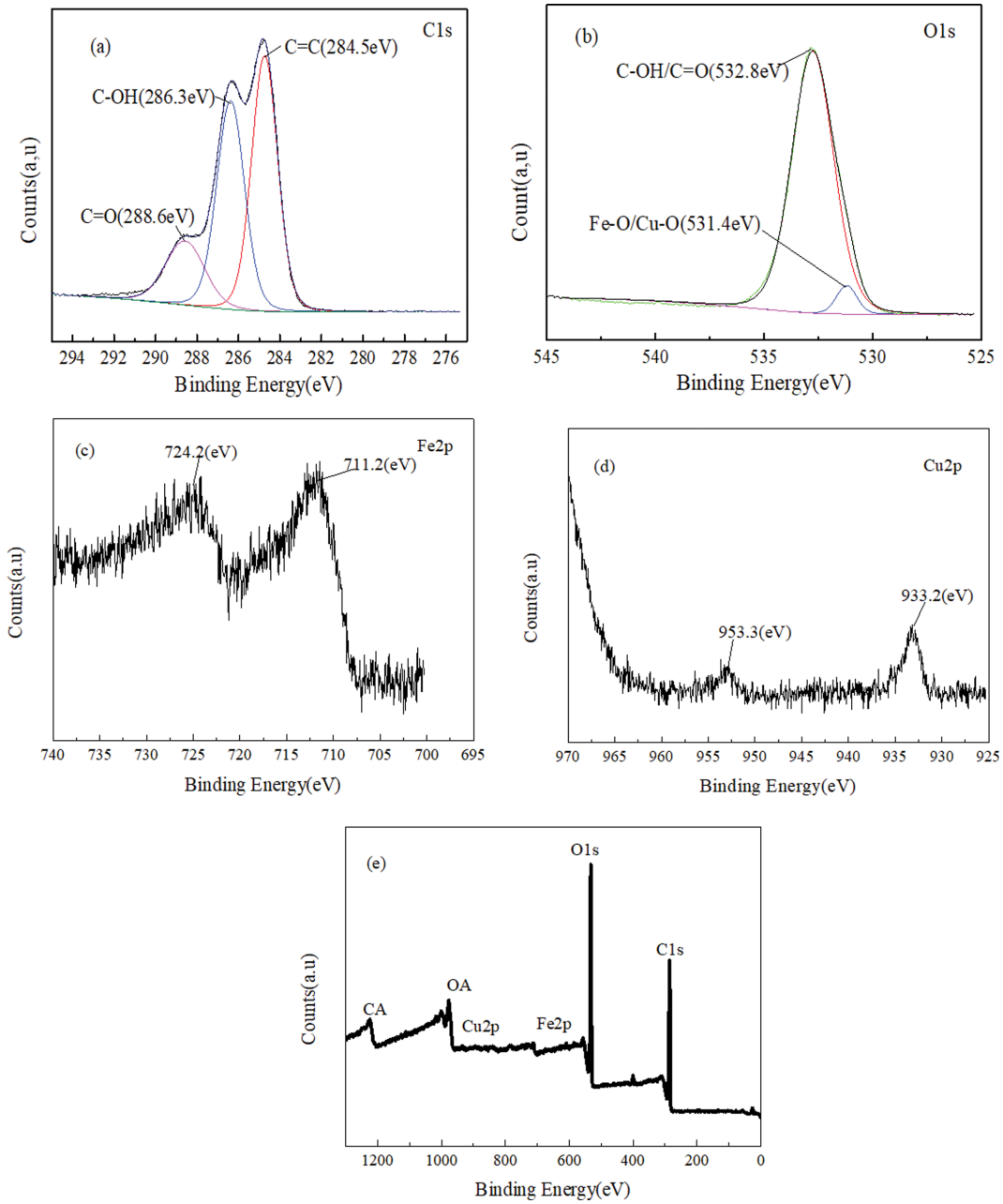

Fig. 3. XPS survey spectrum (a) C 1s; (b) O 1s; (c) Fe 2p; (d) Cu 2p; and (e) survey spectrum.

molecules formed a strong cap on the surface of the Fe/Cu nanocomposites through chemical bonding. The two peaks located at 711.2 eV and 724.2 eV are attributed to Fe 2p3/2 and Fe 2p1/2, respectively, which may belong to iron oxides [25]. In addition, Cu 2p3/2 and Cu 2p1/2 were located at 933.2 and 953.3 eV, respectively, which may be due to Cu^{2+} in CuO [24]. From Fig. 3(e), the Auger electron peaks of C and O were also observed besides photoelectron peaks. Overall, XPS results indicate that the adsorbent surface was covered with biomolecules and citric acid, further confirming that the Fe/Cu nanocomposite was successful synthesized as shown in Fig. 1.

The FTIR spectra of the BM and the Fe/Cu nanocomposites before and after adsorption BM are given in Fig. 4. For BM, the peak at 3,311.12 cm^{-1} was ascribed to N-H stretching vibration [26]. Sharp peak at 1,586.14 cm^{-1} was represented to aromatic rings of BM. The peak at 3,189.59 cm^{-1} and 1,368.34 cm^{-1} corresponded to C-H stretching vibration [27]. As Fig. 4(b) suggested, the band at 3,354.40 cm^{-1} resulted from the O-H stretching vibration or adsorbed water [28]. The peak at 2,935.07 cm^{-1} related to C-H vibration of aliphatic hydrocarbons [23]. At 1,714.48 cm^{-1} was identified C=O stretching vibrations of carboxylic acid [29]. A band at 1,632.46 cm^{-1} was the C=C stretching vibration in the benzene ring, which may be related to the presence of polyphenols in the sweet potato leaf extract [26]. A peak at 619.33 cm^{-1} can be related to Fe-O/Cu-O. From the spectra after BM adsorbed on Fe/Cu nanocomposites, the appearance of new peaks at 3,330.71 and 3,212.36 cm^{-1} indicates that BM molecules were adsorbed on the surface of Fe/Cu nanocomposites. Band at 1,368.83 cm^{-1} was corresponding to C-N stretching vibration for aromatic amines [23]. These changes reveal that the BM was successfully adsorbed on Fe/Cu nanocomposites.

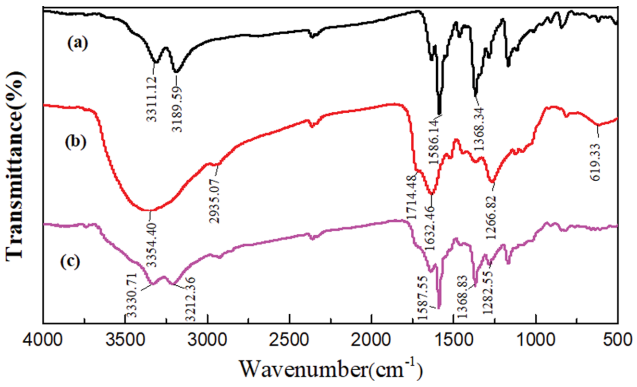

Fig. 4. FTIR spectra of (a) BM, adsorbent (b) before and (c) after adsorption of BM.

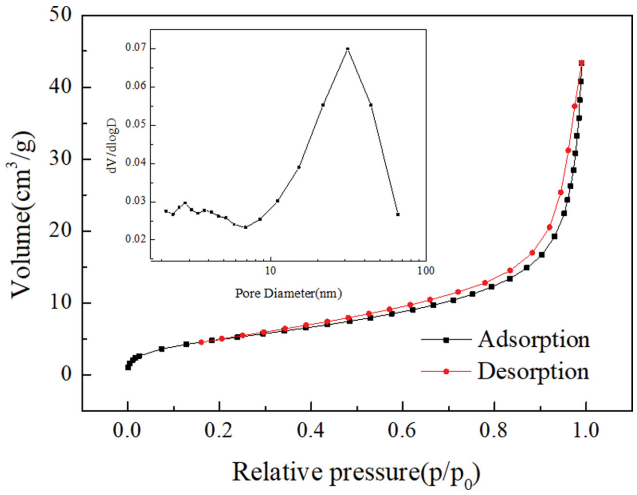

Fig. 5. Nitrogen adsorption-desorption isotherm and the pore size distribution of Fe/Cu nanocomposites.

Nitrogen adsorption-desorption isotherm and the pore size distribution of Fe/Cu nanocomposites are shown in Fig. 5. The isotherm can be defined as type IV isotherm. There was a hysteresis loop at a relative pressure of 0.4-1.0, which indicates that the presence of mesoporous structure [30]. The specific surface area and average pore diameter of the Fe/Cu nanocomposites were 18.49 m^2/g and 14.44 nm, respectively.

2. Model Design of Experiment and Results

2-1. Model Design

The response surface method (RSM) is a practical technique to optimize process conditions [31]. To determine the optimal adsorption conditions and the interaction between various factors, the Box-Behnken Design (BBD) was employed to evaluate the factors

Table 1. Coded levels and values of experimental variables

Experimental variable	Unit	Coded levels and values		
		−1	0	+1
X_1: Adsorption time	min	300	420	540
X_2: Adsorbent dosage	g L^{-1}	0.4	0.5	0.6
X_3: pH		4	5	6

Table 2. Experimental design matrix for adsorption BM

Run	Factors			Adsorption capacity		
	X_1	X_2	X_3	Observed	Predicted	Residual
1	300	0.4	5	151.92	151.27	0.65
2	540	0.4	5	154.15	153.98	0.17
3	300	0.6	5	126.22	126.39	−0.17
4	540	0.6	5	131.98	132.63	−0.65
5	300	0.5	4	129.07	129.29	−0.22
6	540	0.5	4	134.41	134.14	0.27
7	300	0.5	6	135.53	135.8	−0.27
8	540	0.5	6	140.12	139.9	0.22
9	420	0.4	4	146.78	147.22	−0.44
10	420	0.6	4	127.02	126.64	0.38
11	420	0.4	6	155.5	155.89	−0.39
12	420	0.6	6	130.68	130.24	0.44
13	420	0.5	5	143.39	142.3	1.09
14	420	0.5	5	141.8	142.3	−0.5
15	420	0.5	5	143.23	142.3	0.93
16	420	0.5	5	140.69	142.3	−1.61
17	420	0.5	5	142.37	142.3	0.074

including adsorption time (X_1), adsorbent dosage (X_2) and pH (X_3) which affected the adsorption capacity of BM. Three variables with ranges were shown in Table 1.

2-2. Statistical Analysis

Adsorption conditions were optimized by BBD model of RSM. The response variables acquired from 17 groups of experiments are shown in Table 2. The mathematical relationship between response and experimental factor was established by the quadratic polynomial model. The quadratic polynomial equation between adsorption capacity (q) and three variables (X_1-X_3) was used for regression

Table 3. Analysis of variance for adsorption of BM onto Fe/Cu nanocomposites

Source	Sum of squares	Degree of freedom	Mean square	F-value	P-value Prob>F	
Model	1,331.76	9	147.97	153.94	<0.0001	Significant
X_1	40.14	1	40.14	41.76	0.0003	
X_2	1,068.38	1	1,068.38	1,111.42	<0.0001	
X_3	75.34	1	75.34	78.37	<0.0001	
X_1X_2	3.12	1	3.12	3.24	0.1149	
X_1X_3	0.14	1	0.14	0.15	0.7135	
X_2X_3	6.40	1	6.40	6.66	0.0364	
Residual	6.73	7	0.96			
Lack of fit	1.83	3	0.61	0.5	0.7035	Not significant
R-squared	0.995					

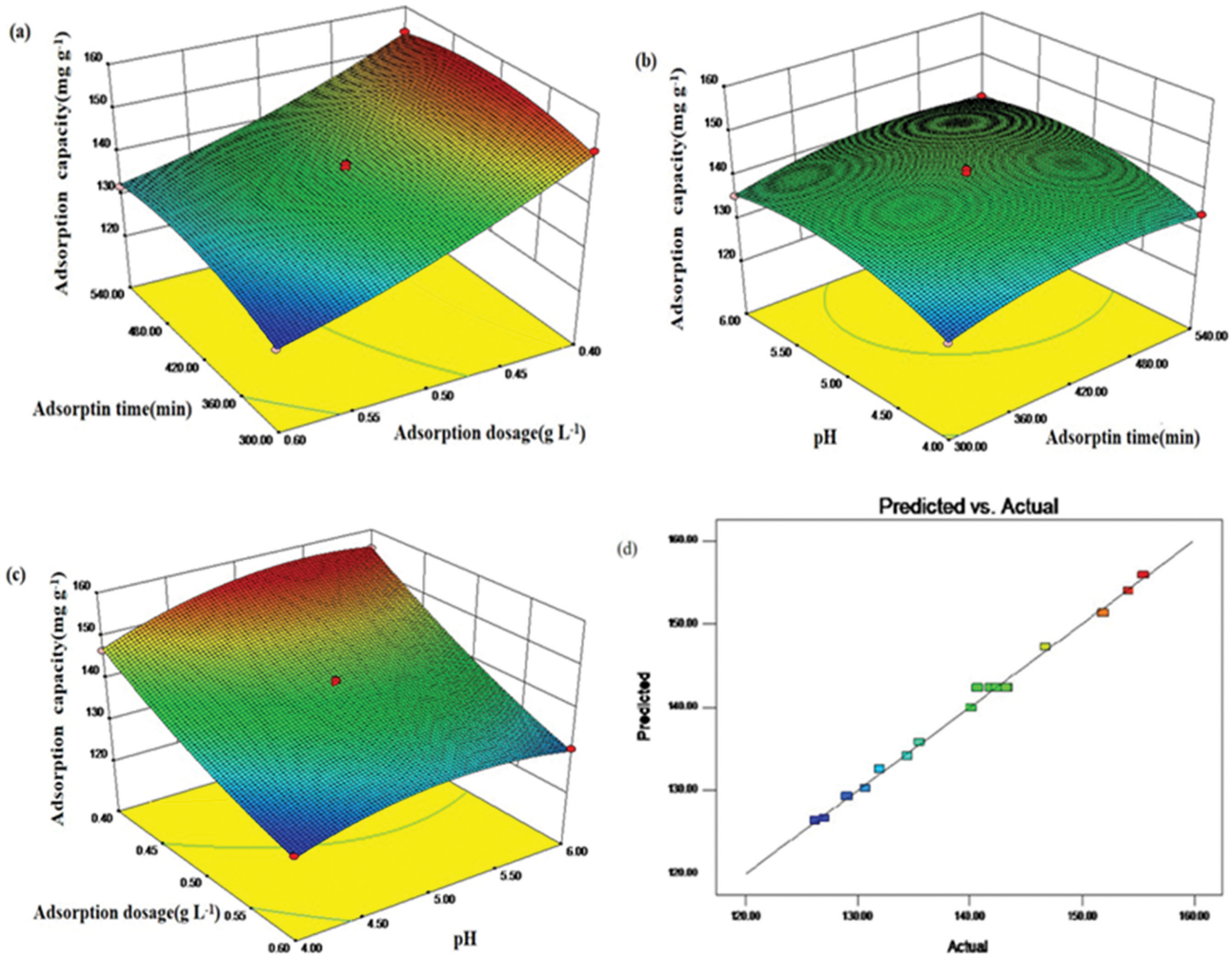

Fig. 6. Three-dimensional response surface plot of adsorption capacity versus (a) adsorption time and adsorbent dosage, (b) adsorption time and pH, (c) adsorbent dosage and pH, (d) the relationship between the predicted and actual values for BM adsorption capacity.

analysis, as follows:

$$q=142.30+2.41X_1-11.56X_2+3.07X_3+0.88X_1X_2-0.19X_1X_3 -1.26X_2X_3-3.22X_1^2+1.99X_2^2-4.29X_3^2 \quad (2)$$

The analysis of variance (ANOVA) was used to assess the applicability of the model. The ANOVA result for BM adsorption is shown in Table 3. The 'Prob>F' less than 0.05 and 'F-value' greater than 5 indicates that the model was significant [32]. From Table 3, the p-value of the model was less than 0.0001 and the value of *F* was 153.94, indicating that the model was significant under selected conditions. The determination coefficient R^2 reached 0.995, implying that the experimental result was consistent with the model. The 'lack of fit' was not significant, which demonstrated that the effect of experimental error could be negligible.

2-3. Response Surface Analysis

RSM was used to assess the relationship between a set of parameters and the observed response to the adsorption capacity of BM, including adsorption time, adsorption dosage and pH. The influence of interaction factors on the response value is illustrated in Fig. 6. According to Fig. 6(a) and (c), the adsorption capacity for BM on per unit mass adsorbent decreased with the increasing adsorbent dosage. The adsorption capacity increased first and then decreased slowly with increasing initial solution pH value, which can be seen from Fig. 6(b) and (c). The results show that the highest BM adsorption efficiency of 157.06 mg/g was obtained at the contact time of 443 min, adsorbent dosage of 0.4 g/L and pH 5.5. To verify the reliability of prediction conditions, five sets of parallel experiments were performed under the optimal conditions. The adsorption capacities were 152.89, 156.37, 160.26, 157.45 and 155.72 mg/g, respectively, which were consistent with the predicted values. The result indicated the good applicability of the model for BM adsorption experiment. Fig. 6(d) was a random scatter plot of the actual values and predicted adsorption capacity of BM onto Fe/Cu nanocomposites; it can be found that the experimental data of BM adsorption was close to the predicted data of the model, indicating that the model can well reflect the experimental data.

3. Isotherm Studies

Adsorption equilibriums are significant for the study of adsorption process, which explored the effect of different temperatures and concentration on adsorption. Sips [33], Langmuir [34], Redlich-Peterson [35] and Freundlich [36] models are utilized to study the isotherm data. The equations are expressed as follows:

Sips isotherm model: $$q_e=\frac{q_{ms}(K_sC_e)^m}{1+(K_sC_e)^m} \quad (3)$$

Langmuir isotherm model: $$q_e=\frac{K_Lq_mC_e}{1+K_LC_e} \quad (4)$$

Redlich-Peterson isotherm model: $$q_e=\frac{A_RC_e}{1+B_RC_e^g} \quad (5)$$

Freundlich isotherm model: $$q_e=K_FC^{1/n} \quad (6)$$

where C_e (mg/L) and q_e (mg/g) are the equilibrium concentration and equilibrium adsorption capacity, respectively. q_{ms} (mg/g) is the saturation adsorption capacity of Sips model and q_m (mg/g) represents the maximum monolayer adsorption capacity of Langmuir model, respectively. K_s (L/mg) and m are the Sips constants. K_L (L/mg) is the Langmuir constant. A_R, B_R and g are the constants of R-P isotherm. K_F ((mg/g)(L/mg)$^{1/n}$) is Freundlich constant. 1/n between 0 and 1, reflects the favorability of adsorption and degree of heterogeneity of the adsorbent surface.

The deviation between experimental data and model data is tested by chi-square. The lower χ^2 implied difference is not significant. Non-linear chi-square is calculated by Eq. (7):

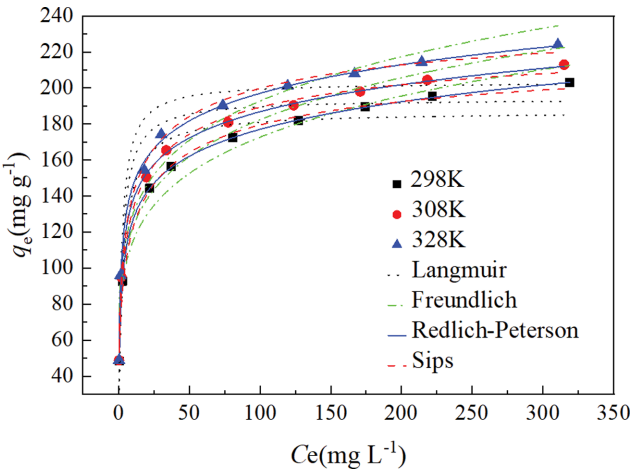

Fig. 7. Nonlinear fitting of experimental data with isotherm models (t=420 min, adsorbent dosage=0.4 g L^{-1}, pH=5.3).

Table 4. Parameters of adsorption isotherm for BM on Fe/Cu nanocomposites

Parameters	298 K	308 K	318 K
Langmuir isotherm			
q_m (mg g^{-1})	186.84	193.95	203.32
K_L (L mg^{-1})	0.31	0.43	0.48
R^2	0.9249	0.9233	0.9181
χ^2	12.27	11.28	13.42
Freundlich isotherm			
K_F ((mg g^{-1})(L/mg)$^{1/n}$)	75.55	81.92	87.71
1/n	0.18	0.17	0.17
R^2	0.9509	0.9447	0.9445
χ^2	12.73	17.21	19.11
Redlich-Peterson isotherm			
A_R	135.57	170.98	205.13
B_R	1.26	1.46	1.68
g	0.89	0.90	0.90
R^2	0.9997	0.9985	0.9978
χ^2	0.03	0.72	1.52
Sips isotherm			
q_{ms} (mg g^{-1})	235.92	243.15	256.73
K_S (L mg^{-1})	0.11	0.14	0.15
m	0.48	0.47	0.47
R^2	0.9953	0.9903	0.9904
χ^2	0.87	2.31	2.49

$$\chi^2 = \sum \frac{(q_{e,exp} - q_{e,cal})^2}{q_{e,exp}} \quad (7)$$

where $q_{e,exp}$ (mg/g) is the experimental adsorption capacity, $q_{e,cal}$ (mg/g) is calculated BM adsorption capacity of each model.

The plots of q_e versus C_e for the adsorption of BM onto Fe/Cu nanocomposites at 298, 308 and 318 K are shown in Fig. 7. The parameters of adsorption isotherm for BM on Fe/Cu nanocomposites are presented in Table 4. With the temperature from 298 to 318 K, the adsorption capacity increased at the same adsorption condition, indicating that the adsorption process may be endothermic.

As for the Redlich-Peterson isotherm model, the values of parameters A_R and B_R both increased with increasing the temperature. Furthermore, the values of g were all lower than 1. The R^2 values of Redlich-Peterson isotherm were higher than 0.99 and the χ^2 values were lower than 1.52. All the parameters manifested that the Redlich-Peterson isotherm model provided a satisfactory fit for the BM adsorption process. R^2 obtained from Sips model was higher than 0.99 and χ^2 were lower than 2.37. The maximum adsorption capacity of BM at 298 K, 308 K and 318 K was 235.92 mg/g, 243.12 mg/g and 256.73 mg/g, respectively. The results suggest that the adsorption process was well represented by Sips isotherm model. But the Langmuir model and Freundlich model were not suitable for the adsorption of BM due to the lower R^2 and the higher χ^2.

The comparison of adsorption capacity of BM on various adsorbents is shown in Table 5. Results show that Fe/Cu nanocomposites prepared from sweet potato leaf extract had higher adsorption capacity for BM and could be considered as a promising adsorbent for the removal of BM.

4. Thermodynamic Properties

To study the influence of temperature on the adsorption process, thermodynamic parameters were calculated, which could predict the feasibility, orientation and spontaneity of the adsorption process. The thermodynamic parameters included Gibbs free energy (ΔG), enthalpy change (ΔH) and entropy change (ΔS). Three parameters were calculated using the following equations [40]:

Table 5. Comparison of adsorption capacity of BM with different adsorbents

Adsorbent	q_e (mg g^{-1})	References
$H_2Ti_3O_7$ titanate nanotubes	68.60	[17]
modified sugarcane bagasse	0.04 mmol/g(13.51)	[37]
modified luffa sponge	88.32	[38]
Al-MCM-41	23.81	[39]
Fe/Cu nanocomposites	235.92	This study

$$K_C = \frac{C_{ad}}{C_e} \quad (8)$$

$$\Delta G = -RT\ln K_C \quad (9)$$

$$\ln K_C = \frac{\Delta S}{R} - \frac{\Delta H}{RT} \quad (10)$$

where C_e and C_{ad} are the BM concentration in solution at equilibrium and the concentration of BM adsorbed at equilibrium, respectively. T represents the temperature in Kelvin, R represents the universal gas constant (8.314 J/(K mol).

The values of ΔG for BM were −12.90, −14.01, −14.94 kJ/mol at 298, 308, 318 K, respectively. The negative values of ΔG revealed that the BM adsorption onto Fe/Cu nanocomposites was feasible experimentally and spontaneous. The value of ΔH was 17.36 kJ/mol confirmed BM adsorption onto Fe/Cu nanocomposites was endothermic and manifested that higher temperature was positive for the adsorption process. The value of ΔS was 0.10 J/(K mol) suggested that the solid-liquid interface chaotic degree was increasing.

5. Kinetics Studies

Kinetics of adsorption is an important parameter in characterizing adsorption efficiency. To understand the characteristics of the adsorption process, the pseudo-first order [41], the pseudo-second order and intra-particle diffusion model were used to define the kinetic behavior [42,43]. The three model equations are as follows, respectively:

Pseudo-first order model: $$q_t = q_e(1 - e^{-k_1 t}) \quad (11)$$

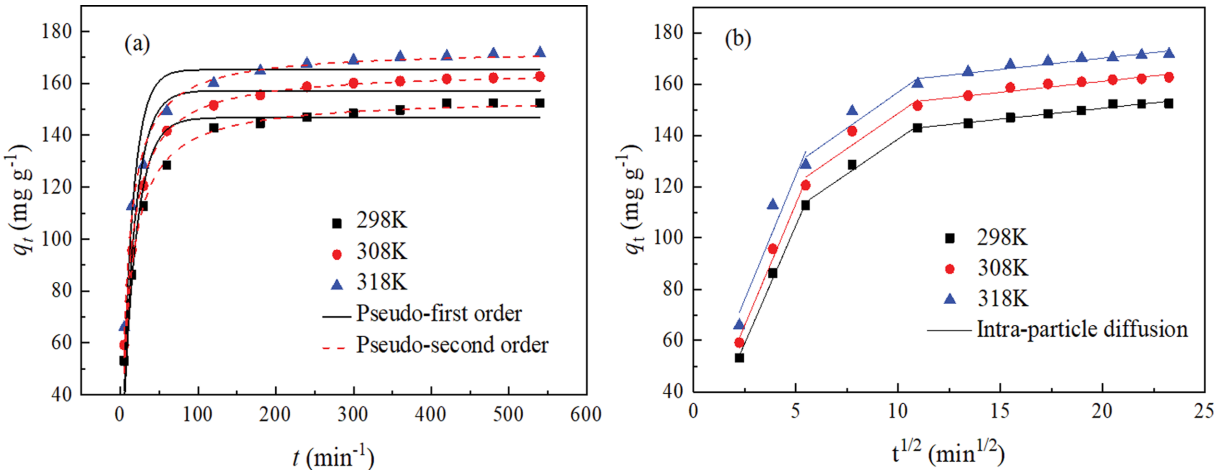

Fig. 8. Regression curves of experimental data for BM adsorption with (a) pseudo first-order, pseudo second-order and (b) intra-particle diffusion kinetic models (adsorbent dosage=0.4 g L^{-1}, BM concentration=100 mg L^{-1}, pH=5.3).

Table 6. Parameters of adsorption kinetic for BM

Model	298 (K)	308 (K)	318 (K)
Pseudo-first-order equation			
k_1 (min^{-1})	0.0577	0.0612	0.0723
q_{cal} (mg g^{-1})	146.82	157.22	165.31
R^2	0.9359	0.9338	0.911
Pseudo-second-order equation			
k_2 (g (mg min)$^{-1}$)	5.90×10^{-4}	5.95×10^{-4}	6.70×10^{-4}
q_{cal} (mg g^{-1})	154.51	165.06	173.12
q_{exp} (mg g^{-1})	152.41	162.68	171.71
R^2	0.9955	0.9963	0.9943
Intra-particle diffusion model			
k_{t1} (mg g^{-1} $min^{1/2}$)	18.38	18.94	19.34
C_1	12.9946	18.6725	27.7399
R	0.9981	0.9943	0.9622
k_{t2} (mg g^{-1} $min^{1/2}$)	5.45	5.50	5.61
C_2	84.1134	93.6186	100.8062
R	0.9919	0.9542	0.9609
k_{t3} (mg g^{-1} $min^{1/2}$)	0.85	0.86	0.88
C_3	133.6363	143.8972	152.4694
R	0.9868	0.9552	0.9519

Pseudo-second order model: $$q_t = \frac{k_2 q_e^2 t}{1 + k_2 q_e t} \quad (12)$$

Intra-particle diffusion model: $$q_t = k_{ti} t^{1/2} + C \quad (13)$$

where k_1 (1/min) and k_2 (g/(mg min)) are the rate constants of pseudo-first order model and pseudo-second order model, respectively; q_e (mg/g) and q_t (mg/g) are the BM adsorption capacity at equilibrium and time t (min), respectively. k_{ti} (mg/(g $min^{1/2}$)) is the intra-particle diffusion rate constant and C (mg/g) is the constant associated with the boundary layer.

The regression curves of kinetic models are illustrated in Fig. 8 and the parameters are given in Table 6. From Fig. 8(a), the adsorption capacity of the Fe/Cu nanocomposites for BM increased and then tended to equilibrium with the extension of time. From Table 6, the correlation coefficient R^2 of the pseudo-first order model was less than 0.94, and the q_{cal} value did not obey the q_{exp} value, which implied that the pseudo-first model was not suitable for the adsorption process. It was clear that the values of q_{exp} agreed with the values of q_{cal} calculated from the nonlinear plots of the pseudo-second order kinetic model, the value of R^2 was greater than 0.99, indicating that the BM adsorption on Fe/Cu nanocomposites was consistent with the pseudo-second-order model.

As shown in Fig. 8(b), the adsorption process had three stages. In the first stage, the adsorption rate was relatively high and the BM molecules were transferred to the external surface of Fe/Cu nanocomposites. The second stage was the intra-particle diffusion process, and the adsorption rate was slow. The third stage was the adsorption equilibrium process. Notably, the k_{t1} of the first stage was much higher than the other two stages, and the $C_1<C_2<C_3$. It was clear that the three lines did not pass through the origin, indicating that the adsorption process was controlled by intra-particle diffusion and boundary layer diffusion.

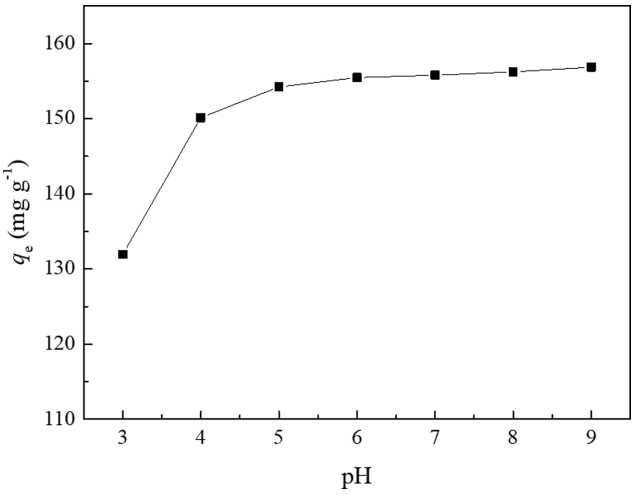

Fig. 9. Effect of pH on adsorption of BM on the Fe/Cu nanocomposites (adsorbent dosage=0.4 g L^{-1}, BM concentration=100 mg L^{-1}).

6. Effects of Solution pH

The pH of the working solution is an important factor affecting the dye adsorption process because it influences surface active sites and surface charge of the adsorbent. The adsorption capacity of BM at different pH is shown in Fig. 9. With the pH from 3 to 5, the adsorption capacity increased significantly. When the pH>5, the adsorption almost reached equilibrium. The point of zero charge (pH_{pzc}) [44] of the Fe/Cu nanocomposites was about 3.6. When the pH was below the pH_{pzc}, the surface charge of Fe/Cu nanocomposites was positive. On the other hand, the surface charge of Fe/Cu nanocomposites was negative, when the solution pH was above the pH_{pzc}. The schematic diagram of the adsorption mecha-

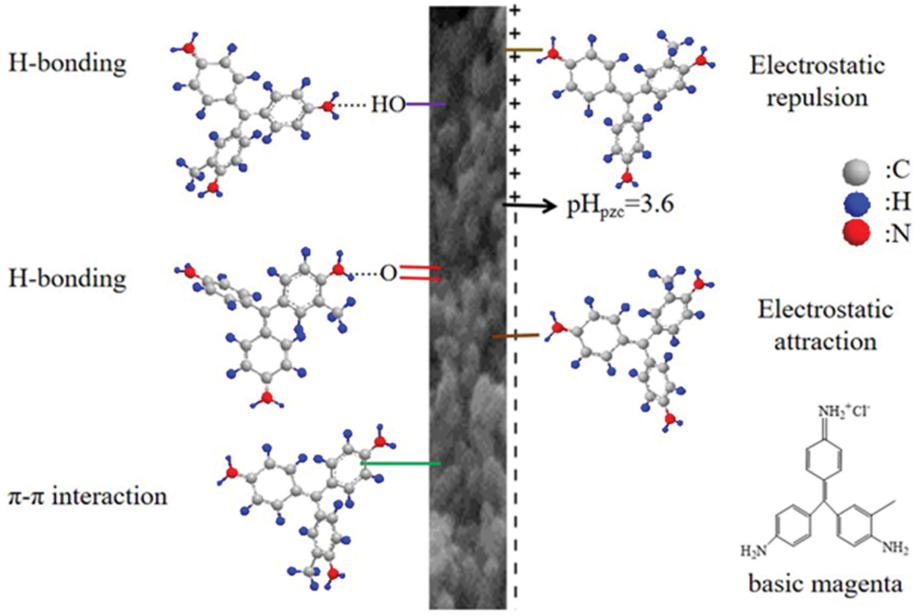

Fig. 10. Schematic diagram of BM adsorption on Fe/Cu nanocomposites.

nism is shown in Fig. 10. When pH<pH_{pzc}, BM adsorption occurred mainly via hydrogen bonding between the amino group of the BM and the hydroxyl of the Fe/Cu nanocomposites as well as via bonding between the amino group of BM and the carbonyl oxygen of the Fe/Cu nanocomposites. In addition, electrostatic repulsion existed between adsorbent and adsorbate. When pH>pH_{pzc}, the surface potential of anion on the adsorbent increased, the electrostatic attraction between Fe/Cu nanocomposites and BM molecules enhanced the adsorption capacity. During the whole BM adsorption process, the π-π interaction and complexation between BM and Fe/Cu nanocomposites also played an important role.

7. Stability

Stability is an important property of adsorbents. The stability of the Fe/Cu nanocomposites was evaluated by comparing the adsorption capacity of fresh and aged samples (Fig. 11). The result showed that the adsorption uptake of all samples remained at around 155 mg/g, indicating that the Fe/Cu nanocomposites were stable over a long period of time.

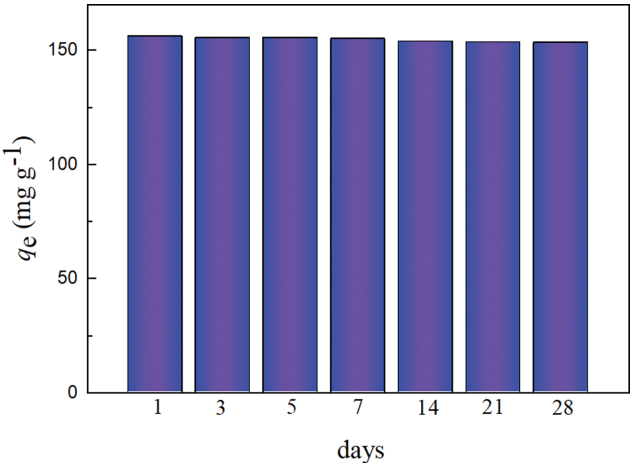

Fig. 11. BM adsorption capacity of Fe/Cu nanocomposites stored openly for 1-28 days.

CONCLUSION

Fe/Cu nanocomposites were synthesized by the green method using sweet potato leaf extracts. The experimental equilibrium data were well described by the Redlich-Peterson model and Sips model, and the maximum monolayer adsorption capacity of Fe/Cu nanocomposites for BM reached 235.92 mg/g at 298 K. By calculating the thermodynamic parameters, the adsorption process was spontaneous and endothermic. The pseudo-second order model proved to be consistent with adsorption kinetic data. The adsorption process of BM onto Fe/Cu nanocomposites was not only controlled by the intra-particle diffusion, but the boundary layer may also have had an effect on the adsorption process. The adsorption of BM was influenced by electrostatic interaction, H-bonding, π-π interaction and complexation. This work promotes the application of renewable resources in the synthesis of new adsorbents and provides a simple and convenient method for the treatment of dye wastewater.

ACKNOWLEDGEMENTS

This project is funded by the Program of Processing and Efficient Utilization of Biomass Resources of Henan Center for Outstanding Overseas Scientists (No. GZS2018004) and Science and Technology Department of Henan Province (No. 162102210002).

REFERENCES

1. R. Zhao, Y. Wang, X. Li, B. Sun and C. Wang, *Appl. Mater. Inter.*, **7**, 26649 (2015).

2. S. Y. Zeng, S. X. Duan, R. F. Tang, L. Li, C. H. Liu and D. Z. Sun, *Chem. Eng. J.*, **258**, 218 (2014).
3. W. Stawinski, A. Wegrzyn, T. Danko, O. Freitas, S. Figueiredo and L. Chmielarz, *Chemosphere*, **173**, 107 (2017).
4. J. W. Fu, Z. H. Chen, M. H Wang, S. J. Liu, J. H. Zhang, J. N. Zhang, R. P. Han and Q. Xu, *Chem. Eng. J.*, **259**, 53 (2015).
5. C. C. Ye, F. Y. Zhao, J. K. Wu, X. D. Weng, P. Y. Zheng, Y. F. Mi, Q. F. An and C. J. Gao, *Chem. Eng. J.*, **307**, 526 (2017).
6. X. Z. Wei, X. Kong, C. T. Sun and J. Y. Chen, *Chem. Eng. J.*, **223**, 172 (2013).
7. P. Zhang, I. Lo, D. O'Connor, S. Pehkonen, H. F. Cheng and D. Y. Hou, *J. Colloid. Interface Sci.*, **508**, 39 (2017).
8. W. Stawinski, O. Freitas, L. Chmielarz, A. Wegrzyn, K. Komedera, A. Błachowski and S. Figueiredo, *Chemosphere*, **153**, 115 (2016).
9. A. Ayati, M. N. Shahrak, B. Tanhaei and M. Sillanpaa, *Chemosphere*, **160**, 30 (2016).
10. Y. Zhou, Y. He, Y. Xiang, S. Meng, X. Liu, J. Yu, J. Yang, J. Zhang, P. Qin and L. Luo, *Sci. Total Environ.*, **646**, 29 (2019).
11. Y. Liu and D. Z. Sun, *J. Hazard. Mater.*, **143**, 448 (2007).
12. S. K. Bhunia and N. R. Jana, *Appl. Mater. Inter.*, **6**, 20085 (2014).
13. S. W. Peretti, C. J. Tompkins, J. L. Goodall and A. S. Michaels, *J. Membr. Sci.*, **195**, 193 (2001).
14. J. H. Mo, Y. H. Lee, J. Kim, J. Y. Jeong and J. Jegal, *Dyes Pigm.*, **76**, 429 (2008).
15. J. Li, J. Cai, L. Zhong, H. L. Cheng, H. Wang and Q. M. Ma, *Appl. Clay Sci.*, **167**, 9 (2019).
16. L. H. Huang, J. J. Kong, W. L. Wang, C. L. Zhang, S. F. Niu and B. Y. Gao, *Desalination*, **286**, 268 (2012).
17. H. R. Mariana, C. S. Roberto and F. Ruiz, *Micropor. Mesopor. Mater.*, **276**, 183 (2019).
18. L. Wang, X. L. Wu, W. H. Xu, X. J. Huang, J. H. Liu and A. W. Xu, *Appl. Mater. Inter.*, **4**, 2686 (2012).
19. A. S. Prasad, *Mater. Sci. Semicond. Process*, **53**, 79 (2016).
20. R. K. Das, B. B. Borthakur and U. Bora, *Mater. Lett.*, **64**, 1445 (2010).
21. F. Luo, D. Yang, Z. L. Chen, M. Megharaj and R. Naidu, *J. Hazard. Mater.*, **296**, 37 (2015).
22. T. Shahwan, S. A. Sirriah, M. Nairat, E. Boyacı, A. E. Eroglu, T. B. Scott and K. R. Hallam, *Chem. Eng. J.*, **172**, 258 (2011).
23. T. Wang, X. Y. Jin, Z. L. Chen, M. Megharaj and R. Naidu, *Sci. Total. Environ.*, **466**, 210 (2014).
24. P. Zhang, D. Y. Hou, D. O'Connor, X. R. Li, S. Pehkonen, R. S. Varma and X. Wang, *Sustainable. Chem. Eng.*, **6**, 9229 (2018).
25. T. Yamashita and P. Hayes, *Appl. Surf. Sci.*, **254**, 2441 (2008).
26. X. L. Weng, M. Y. Guo, F. Luo and Z. L. Chen, *Chem. Eng. J.*, **308**, 904 (2017).
27. E. J. Lara-Vásquez, M. Solache-Ríosb and E. Gutiérrez-Segura, *J. Environ. Chem. Eng.*, **4**, 1594 (2016).
28. Y. F. Wei, Z. Q. Fang, L. C. Zheng and E. P. Tsang, *Appl. Surf. Sci.*, **299**, 322 (2017).
29. G. Vazquez, E. Fontenla, J. Santos, M. S. Freire, J. Gonzalez-Alvarez and G. Antorrena, *Ind. Crop. Prod.*, **28**, 279 (2008).
30. A. Wei, B. Liu, H. Zhao, Y. Chen, W. L. Wang, Y. Ma, H. Q. Yang and S. Z. Liu, *Chem. Eng. J.*, **239**, 141 (2014).
31. S. Yavari, A. Malakahmad, N. B. Sapari and S. Yavar, *Process Saf. Environ. Prot.*, **109**, 509 (2017).
32. Y. B. Wan, X. Liu, P. L. Liu, L. Zhao and W. H. Zou, *Sci. Total. Environ.*, **639**, 428 (2018).
33. J. L. Wang, and X. Guo, *Chemosphere*, **258**, 127279 (2020).
34. T. Zhou, L. Fang, X. Wang, M. Han, S. Zhang and R. Han, *Desalin. Water Treat.*, **70**, 294 (2017).
35. O. Hamdaoui and E. Naffrechoux, *J. Hazard. Mater.*, **147**, 401 (2007).
36. K. Y. Foo and B. H. Hameed, *Chem. Eng. J.*, **156**, 2 (2010).
37. J. X. Yu, J. Zhu, L. Y. Feng and R. A. Chi, *J. Colloid Interface Sci.*, **451**, 153 (2015).
38. S. F. Li, M. Tao and Y. D. Xie, *Desalin. Water. Treat.*, **57**, 1 (2015).
39. Y. Guan, S. M. Wang, X. Wang, C. Sun, Y. B. Wang and L. J. Hu, *Micropor. Mesopor. Mater.*, **265**, 266 (2018).
40. Y. Liu, *J. Chem. Eng. Data*, **54**, 1981 (2009).
41. J. L. Wang and X. Guo, *J. Hazard. Mater.*, **390**, 122156 (2020).
42. X. Guo and J. L. Wang, *J. Mol. Liq.*, **288**, 111100 (2019).
43. X. Y. Zhang, J. Zhou, Y. B. Fan and J. Y. Liu, *Korean J. Chem. Eng.*, **37**, 1445 (2020).
44. E. J. Lara-Vásquez, M. Solache-Ríos and E. Gutiérrez-Segura, *J. Environ. Chem. Eng.*, **4**, 1594 (2016).